Assessing the combination of magnetic field stimulation, iron oxide nanoparticles, and aligned electrospun fibers for promoting neurite outgrowth from dorsal root ganglia in vitro

Jessica Funnell, Alexis Ziemba, James Nowak, Hussein Awada, Nicos Prokopiou, Johnson Samuel, Yannick Guari, Benjamin Nottelet, Ryan Gilbert

HAL Id: hal-03334562

https://hal.umontpellier.fr/hal-03334562v1

Submitted on 16 Aug 2022

Assessing the combination of magnetic field stimulation, iron oxide nanoparticles, and aligned electrospun fibers for promoting neurite outgrowth from dorsal root ganglia in vitro

Jessica L. Funnell[1], Alexis M. Ziemba[1], James Nowak[2], Hussein Awada[3,4], Nicos Prokopiou[1], Johnson Samuel[2], Yannick Guari,[4] Benjamin Nottelet[3], Ryan J. Gilbert[1]*

Affiliations: [1]Biomedical Engineering, Rensselaer Polytechnic Institute, Troy, NY; [2]Mechanical, Aerospace, and Nuclear Engineering, Rensselaer Polytechnic Institute, Troy, NY; [3]IBMM, Université de Montpellier, CNRS, ENSCM, Montpellier, France; [4]ICGM, Univ. Montpellier, CNRS, ENSCM, Montpellier, France

*Corresponding Author:

Ryan J. Gilbert
Department of Biomedical Engineering
Rensselaer Polytechnic Institute, 110 8th Street, Troy, New York 12180
Email: gilber2@rpi.edu

Abstract

Magnetic fiber composites combining superparamagnetic iron oxide nanoparticles (SPIONs) and electropsun fibers have shown great promise in tissue engineering fields. Controlled grafting of SPIONs to the fibers post-electrospinning generates biocompatible magnetic composites without altering desired fiber morphology. Here, we investigate the potential of SPION-grafted scaffolds to synergistically interact with magnetic fields to promote axonal regeneration. We assessed neurite outgrowth (length and area coverage) from primary rat dorsal root ganglia (DRG) cultured on aligned control and SPION-grafted electrospun fibers. Additionally, we cultured DRG on control fibers incubated with untethered SPIONs to determine how an external magnetic field induces changes in cell behavior when SPIONs are immobilized to a surface compared to dispersed in the culture media. To determine the optimal magnetic field stimulation to promote neurite outgrowth, we generated a static, alternating, and linearly moving magnet and characterized the magnetic flux density at different areas of the scaffold over time. We show that an alternating magnetic field increases neurite length on control and SPION-grafted fibers compared to a static magnetic field. Additionally, both neurite length and area coverage were increased on SPION-grafted fibers compared to cells cultured on control fibers with untethered, dispersed SPIONs added to the culture media. These findings show the potential of combining magnetic field stimulation with magnetic fiber composites for neural regeneration applications.

Statement of Significance
Keywords
Abbreviations

1. Introduction

Aligned electrospun fibers have shown promise for promoting axonal regeneration after nervous system injury in preclinical models; however, the contact guidance provided by aligned fiber scaffolds is not enough to induce full functional recovery [1–4]. Therefore, new strategies for enhancing fibers, like incorporating therapeutics, growth factors, or biocompatible surface coatings, are being researched to provide more robust regeneration after nervous system injury [5]. One area of research that is being further investigated is the use of magnetic fields to stimulation neuronal growth. Several studies have shown that low frequency (<50 Hz) pulsed magnetic fields alone can increase neurite length in vitro [6–9]. Even more recently, studies have investigated utilizing magnetic nanoparticles (MNP) to synergistically provide magnetic field stimulation with mechanostimulation using the particles to non-invasively guide axonal regeneration [10]. Superparamagnetic iron oxide nanoparticles (SPIONs) are the most common magnetic material used in biomedical applications because of their biocompatibility and superparamagnetic properties. Riggio et al. showed that nerve growth factor (NGF)-conjugated SPIONs added to neuron-like cells direct neurite outgrowth in the direction of a static magnetic field [11]. The concept of using MNPs with an external magnetic field to stimulate and/or direct neurite growth in a desired direction has since been explored in numerous studies [12–14]. A study by Yuan et al. compared different types of magnetic fields; a static and alternating magnetic field both increased neurite outgrowth when neuron-like cells were incubated with

2

gold-coated SPIONs, but the alternating magnetic field increased neurite length more than the static field [15]. Overall, these studies highlight how SPIONs can be manipulated with different strengths and types of magnetic fields (static, pulsed, alternating) to cause a variety of effects on neurons. However, this work is largely preliminary and there is a lack of knowledge on optimizing these different parameters to promote neural regeneration.

Because of the promising effects of aligned electrospun fibers and magnetic field stimulation on axonal regeneration, a compelling next step is to combine MNPs with electrospun fibers to create paramagnetic composite scaffolds. These types of composites have been explored for several different biomedical applications, including MRI visualization [16], hyperthermia cancer treatment [17,18], on-demand drug release [19], and bone regeneration/tissue engineering applications [20–22]. SPION incorporation into electrospun fibers is most often accomplished by either blending pre-synthesized SPIONs into the polymer solution prior to electrospinning, including a precursor into the spinning solution that yields SPIONs after a post-electrospinning process, or in-situ synthesis of SPIONs during electrospinning. Only one previous study utilized magnetic composite electrospun fibers for neural regeneration applications. Johnson et al. blended SPIONs into the electrospinning solution to generate aligned magnetic fibers that were then fabricated into injectable conduits that could be oriented in a viscous solution using an external magnet [23]. However, the effect of magnetic field stimulation in combination with the magnetic fibers on neurite outgrowth was not investigated, and the maximum SPION loading percentage that could be used before fiber diameter and alignment was affected was only 6 w/w% SPIONs/polymer. Blending SPIONs into electropsun fibers can often result in unwanted changes in size, shape, and mechanical properties of the fibers compared to unloaded fibers [16].

3

An alternative synthetic approach for generating magnetic fiber composites is to immobilize SPIONs at the polymer surface post-electrospinning. We previously created a SPION-grafting procedure that immobilizes a uniform distribution of SPIONs to the surface of aligned poly-L-lactic acid (PLLA) electrospun fibers without altering the fiber diameter or density, an improvement to previous methods of grafting that used reaction conditions incompatible with biocompatible polymers and had poor control of SPION aggregation. These SPION-grafted fibers were nontoxic to cells and could be easily visualized with MRI after implantation into rats [24]. Here, we investigate further and explore the potential of the SPION-grafted scaffolds to synergistically interact with magnetic fields to promote axonal regeneration. We assessed neurite outgrowth (length and area coverage) from primary rat dorsal root ganglia (DRG) cultured on aligned control PLLA and SPION-grafted PLLA electrospun fibers. Additionally, we cultured DRG on control PLLA fibers incubated with untethered SPIONs to determine how an external magnetic field induces changes in cell behavior when SPIONs are immobilized to a surface compared to dispersed in the culture media. To determine the optimal magnetic field stimulation to promote neurite outgrowth, we generated a static, alternating, and linearly moving magnet and characterized the magnetic flux density at different areas of the scaffold over time. To our knowledge, this is the first study to examine the effects of different types of magnetic fields on neurite outgrowth from neurons cultured on electrospun fibers, as well as the first study to investigate the effect of magnetic composite fibers on neurite outgrowth. We show that an alternating magnetic field increases neurite length on control and SPION-grafted fibers compared to a static magnetic field. Additionally, both neurite length and area coverage were increased on SPION-grafted fibers compared to cells cultured on control fibers with untethered, dispersed SPIONs added to the culture media. These findings show the potential

4

of combining magnetic field stimulation with magnetic fiber composites for neural regeneration applications.

2. Materials and Methods

2.1. Materials

All information on materials and equipment is listed in the Supplementary Information (Table S1 & S2).

2.2. Electrospun Fiber Scaffold Fabrication.

Aligned electrospun fiber scaffolds were prepared as described previously [25,26]. Briefly, an 8 w/w% solution of PLLA in chloroform was prepared and incubated on a stir plate to homogenize for at least 1 h. The solution was then loaded into a 5-mL syringe equipped with a 23-G needle and placed into a syringe pump. Electrospinning was conducted using the parameters listed in Table 1. Electrospun fibers were collected onto 15 x 15 mm glass coverslips secured to the rotating mandrel with double-sided tape for 18 min to produce a dense mat of aligned fibers. To remove the fiber scaffolds, the fibers along the edges of the coverslips were cut with a razor blade and the coverslips were removed from the mandrel with forceps.

To prevent the fibers from lifting off the coverslips during the chemical processing procedure used to graft the SPIONs to the fibers (described in section 2.4), the edges of the scaffold were dipped in a 4 w/w% PLLA/chloroform solution. The dipped scaffolds were dried at room temperature for at least 24 h before use. Both SPION-grafted fiber scaffolds and control

PLLA fiber scaffolds were dip-coated to keep this processing consistent between control and experimental groups.

Table 1. Electrospinning parameters.

PLLA w/w% in Solvent	Solvent	Relative Humidity during Electrospinning	Fiber Collection Time	Fiber Collection Distance	Applied Voltage	Solution Flow Rate	Wheel Rotation Speed
8%	Chloroform	21% ± 1%	18 min	4 cm	15 kV	2 mL/h	1000 rpm

2.3. Iron Oxide Nanoparticle Fabrication

Oleic acid-functionalized SPIONs were synthesized using methods previously described [24]. Briefly, 0.18 g of FeOOH fine powder, 3.2 g of oleic acid, and 5.0 g of n-docosane were combined and evacuated for 30 min. The mixture was then heated under argon at 340°C for 1.5 h. The mixture was then cooled to 50°C and diluted with 15 mL pentane. The nanoparticles were purified using successive dispersion-centrifugation cycles in diethyl ether/ethanol mixtures at a ratio of 2:1 and then 1:1 at 2000 rpm for 10 min with removal of the supernatant. The purification was repeated several times until the supernatant solution became colorless. The remaining solvent was lyophilized and the SPIONs were resuspended in cyclohexane at 10 mg/mL in the presence of oleylamine (200 µL) and freshly used in the grafting procedure.

2.4. Preparation of SPION-Grafted Fiber Composites

SPION-grafted fiber composites were fabricated as previously described [24] but with a few modifications so that more scaffolds could be functionalized at once and so that SPION aggregation was minimized. To prepare the SPION-grafted fiber composites, the first step is propargylation of the PLLA fibers. In a flamed-dried 3-neck lab reactor (1L) with lid and steel

clamp, 600 mL of dry Et$_2$O was introduced under argon atmosphere and the medium was cooled to −78 °C. Then, two custom-made Teflon molds (see <mark>SI Figure XX</mark>) holding 18 PLLA fiber scaffolds on glass coverslips were immersed into the solvent. The solution was saturated with argon (15 min bubbling of Ar gas) and then an LDA (Lithium diisopropylamide) solution (2M, 1 mL, 2 mmol) was added. After 15 min, a propargyl bromide solution (80 wt% in toluene, 0.5 mL, 4.5 mmol) saturated with with argon was injected, and the mixture was stirred for an additional 15 min at −78°C. The samples were washed several times in a cold diethyl ether bath for 30 min, before drying under air atmosphere.

The PLLA fibers are then functionalized with phosphonic acid through thiol-yne photo addition. In the flamed-dried 3-neck lab reactor (1L) with lid and steel clamp protected from light and placed under argon atmosphere, 12-mercaptododecylphosphonic acid (6 mg, 2x10^{-5} mol) dissolved in 600 ml of a 3:1 cyclohexane/acetone mixture were added. Then, the two Teflon molds holding 18 scaffolds with propargyl-functionalized PLLA fibers were immerged into the solvent. The solution was saturated with argon prior to the addition of the photoinitiator DMPA (6 mg, 2.3x10^{-5} mol) and protected with two balloons containing argon gas. Then UV irradiation (100 mW.cm^{-2}) was carried out for both sides of the Teflon molds for 10 min under gentle stirring at room temperature. Following the thiol-yne photo-addition, PLA fibers were washed several times in cyclohexane and dried under air atmosphere.

SPION-grafted PLLA fibers were then fabricated through a free ligand exchange procedure. First, 2 mL of freshly prepared oleic acid-functionalized SPIONS (10 mg/ml) were diluted in 600 mL of cyclohexane and sonicated for 1h. The solution mixture was introduced into the flamed-dried 3-neck lab reactor (1L) with lid and steel clamp under air atmosphere. Then, the two Teflon molds holding 18 scaffolds of the phosphonic acid functionalized PLLA fibers were

immerged into the solvent. The reaction was protected from light and stirred for 12 h at room temperature. The SPION-grafted PLA fibers were cleaned by successive washing in a cyclohexane solution and dried under air. Each scaffold was then sonicated in ethanol for 30 s, repeated 5 times with the ethanol replaced each time. An additional 3 ethanol washes (no sonication) was performed and the scaffolds were dried either in a cell culture hood to be used for cell experiments or just on the benchtop for scaffold characterization experiments. A change in the color of the PLLA fibers was clearly observable from white to light brown (SI XXX). Any scaffold not used for cell experiments was stored in the fridge after drying until further characterizations.

2.5. Scanning Electron Microscopy and Fiber Morphological Characterization

Scaffolds were secured to a square SEM stub using carbon tape. A ~0.5-nm layer of Au/Pd was sputter coated onto the fiber scaffolds using a Technics Hummer V Sputter Coater. A FEI Versa 3D Dual Beam SEM was used to acquire 4-6 images at both a low (2000x) and high (15,000x+) magnification at different locations on the scaffold. The following imaging parameters were used: 5.0 kV accelerating voltage, 10 mm working distance, 5.0 nm spot size, and 30 µm aperture. At least one scaffold per material fabrication batch, considered one material replicate, was imaged for each group: n=6 control PLLA fiber batches and n=5 SPION-grafted fiber batches.

2.5.1. Fiber Diameter and Density Analysis

Low magnification images were used to analyze fiber diameter and density with ImageJ software (NIH). For fiber diameter, the line tool was used to draw a line over the width of the fiber and its length was recorded. All fibers whose entire width was visible were analyzed in each image (overlapped fibers were excluded). A minimum of 50 fibers were analyzed per each

material replicate. For fiber density, the width of each image in microns was recorded, and then the number of fibers in the image was manually counted (including overlapped fibers). The number of fibers was then divided by the length of the image to give a fiber density. A total of 4-6 images was analyzed per material replicate.

2.5.2. Fiber Alignment Analysis

Low magnification images were used to analyze fiber alignment with the Fast Fourier Transform (FFT) function in ImageJ. The oval profile plugin was used to analyze pixel intensity in radial sums from the FFT output image and these data were normalized using a peak normalization method, where the maximum pixel intensity and corresponding angle is set to 1 and 0, respectively [27]. A minimum number of 4 images were analyzed per material replicate, with n=6 total material replicates for control PLLA fiber batches and n=5 SPION-grafted fiber batches. Plots of the angle deviation from the maximum intensity angle according to the normalized FFT data were generated and the area under the curve was used for statistical analysis to compare alignment of control PLLA and SPION-grafted PLLA fibers.

2.5.3. SPION Grafting Density Analysis

High magnification images were used to analyze the density of SPIONs on the fibers after the grafting procedure. The image was loaded into ImageJ software and the scale was set accordingly. A ~2 μm^2 box was drawn over a fiber where there were no large aggregates of SPIONs because it is impossible to discern individual nanoparticles in the aggregates. The exact area of the box and the number of SPIONs in the box was then recorded. A minimum of one box was drawn and analyzed per each image, with a minimum of 4 images analyzed per material replicate and n=5 SPION-grafted fiber replicates.

2.5.4. SPION Aggregate Analysis

Low magnification images were used to analyze SPION aggregates on the scaffold after the grafting procedure. An aggregate was defined as a collection of SPIONs with an area greater than 0.5 μm^2. The image was loaded into ImageJ software and the scale was set accordingly. The number and area of each aggregate along a completely visible fiber (in the foreground of the image) was analyzed for a minimum of 3 fibers per image and at least 4 images were analyzed per material replicate, with n=5 SPION-grafted fiber replicates.

2.6. Electrospun Fiber Surface Wettability Assessment

Surface wettability of control PLLA fiber and SPION-grafted PLLA fiber scaffolds was assessed using a Kruss DSA 100 goniometer as described previously [25]. Briefly, a 3-µL droplet of diH20 was placed on the fibers and an image was captured orthogonal to the orientation of the aligned fibers. Three droplets were assessed in three areas on a scaffold. The static water contact angle was then assessed from droplets for n=3 control PLLA and SPION-grafted PLLA fiber scaffolds.

2.7. Magnet/Culture Configuration and Magnetic Field Simulations

All magnets used in each of the three magnetic field setups are N52 grade (1.43 T), ½ in. diameter by 3/8 in. long neodymium cylinder magnets. An image of each magnetic field setup is shown in Figure S1 in Supporting Information. The static magnetic field condition consisted of a single magnet in a well of a 12-well plate (Corning). The magnet was secured in the well with its face centered to an adjacent well by covering it with a mixture of polydimethylsiloxane (PDMS) with a 1:10 ratio of curing agent to silicone elastomer (Dow SYLGARD™ 184 kit). This ensures that there was a 10-mm distance from the pole of the magnet and the edge of a scaffold placed in the adjacent well. A maximum of two magnets were used per well plate, with each one on opposite sides so that the magnetic field strength is negligible at the second scaffold in the plate (Figure 1A).
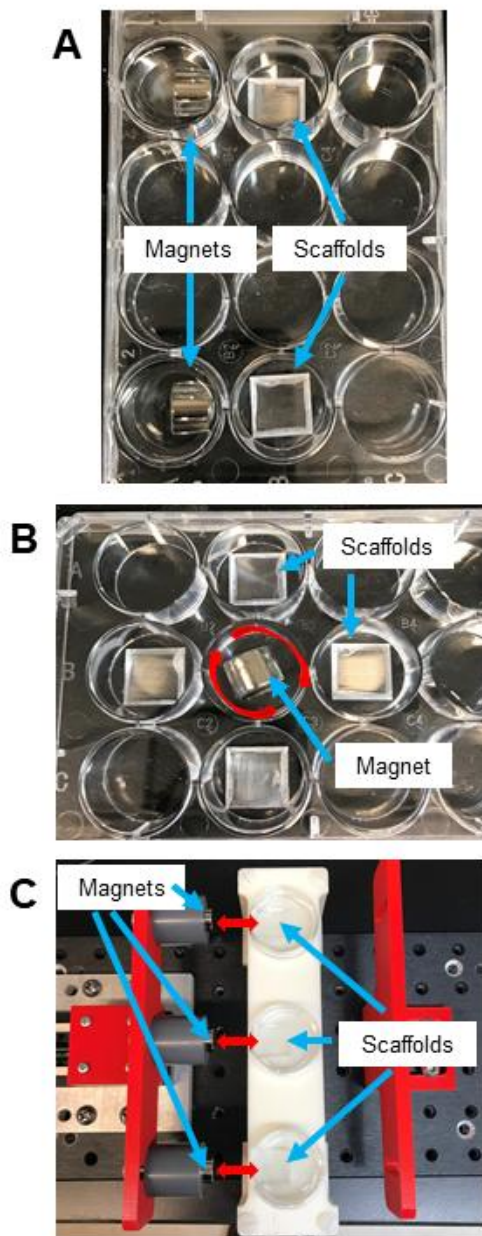
The alternating magnetic field was generated by placing a single magnet in well 2B and placing the entire well plate on a magnetic stir plate (Figure 1B). The magnet was rotated at a speed of 360º/second or one full rotation per second. A maximum of 4 scaffolds were placed in the wells directly adjacent to the magnet (not diagonal) so that the distance between the pole of the magnet and the edge of the scaffold was 10 mm.

To determine if a dynamic "pulling" on the fibers with a magnetic field would affect neurite outgrowth differently from the alternating or static magnetic field, the magnet was moved back and forth from the scaffold to create a linearly moving magnetic field. An electronic linear motion stage was fabricated in house to provide constant motion of a magnet to and from a stationary platform that housed a 35-mm diameter petri dish. The translation stage and controller (ThorLabs, USA, # MTS50/M-Z8) allowed for a maximum magnet spacing of 50 mm, and a maximum linear speed of 2.4 mm/s and repeatability of ± 1.6 μm. After initial pilot tests

Figure 1: Magnetic field configurations. A) Static magnetic field configuration where two magnets are placed on opposite sides of a 12-well plate and scaffolds are placed adjacent to the magnet pole. B) Alternating magnetic field configuration where magnet spins (motion indicated by red arrows) in the center well and four scaffolds are placed around the magnet in adjacent wells. C) Linearly moving magnetic field configuration where three separate scaffolds in petri dishes sit on a stage where magnets move 10 mm back and forth from the scaffolds at 2 mm/s.

with cells to determine the most effective results, all experiments with the linearly moving magnetic field utilized the following parameters: total travel distance of 10 mm moving at a constant speed of 2 mm/s. The minimum distance between the scaffold in the petri dish and the magnet was 10 mm, to be consistent with the alternating and static magnetic field conditions. The stage allowed 3 magnets to move back and forth from three separate petri dishes (Figure 1C). To prevent the scaffolds from floating/moving around in the petri dish (normally prevented by the size of the well in a 12-well plate), a thick layer of PDMS was cured in the dishes and a square of PDMS was cut out by the side of the dish to allow a scaffold to be placed in the cutout. All well plates and petri dishes were sterilized with 70% ethanol and dried overnight in a cell culture hood before use with cells. The linear motion stage setup was sterilized with ethanol before being placed in a cell culture incubator (37°C, 5% CO_2).

2.7.1. Magnetic Field Simulations

Magnetic field simulation software (Quickfield^{TM}, USA) was used to estimate the magnetic field flux density as a function of magnet spacing in relation to the scaffolds in the petri dishes. The strength of the magnet was set at 1.480 T based on manufacturer data sheets, while the relative permeability of the field between the magnets was set at 1.0. A color map and graphs of the magnetic field flux density over time at specific locations on the scaffold were generated using the data values from the 2D simulation.

2.8. SPION-Grafted Fiber Incubation in Magnetic Fields

To determine if the magnetic fields themselves altered the morphology of the SPION-grafted fiber scaffolds, scaffolds were placed in deionized water in each of the magnetic field setups: static magnetic field, alternating magnetic field, and linearly moving magnetic field. Scaffolds incubated with no magnetic field present were used as a control. All scaffolds were incubated for 48 h to mimic the timeline of the cell experiments. The scaffolds were then air-dried overnight and prepared for SEM as described in section 2.5 above. SEM was used to acquire 4-6 images at both a low (2000x) and high (15,000x+) magnification at different locations on the scaffold (same imaging parameters as section 2.5). Three scaffolds from different grafting fabrication batches were used for each magnetic field type to obtain images in triplicate. Fiber alignment was analyzed as described in section 2.5.2. above.

2.9. Fiber Scaffold Preparation for Cell Culture

All electrospun fiber scaffolds were sterilized with ethanol and dried overnight in a cell culture hood before use in cell experiments. Scaffolds were then coated with 10 ug/mL laminin for at least one hour and then washed three times with deionized water before DRG were seeded onto the scaffolds.

2.10. DRG Isolation and Culture

All procedures were approved by the Rensselaer Polytechnic Institute IACUC. DRG were isolated from two-day old Sprague Dawley rats using a protocol described previously [25,28]. The DRG were then stored in F12 on wet ice before plating onto the electrospun fiber scaffolds. DRG isolated from one animal were considered one biological replicate and at least n=3 biological replicates were used for all cell experiments.

The DRG were removed from the F12 and placed in the center of each electrospun fiber scaffold using fine forceps. Neuron growth media, consisting of neural basal media containing with 50 ng/mL nerve growth factor, B-27 supplement (2% v/v), 0.5 mM L-glutamine, and penicillin-streptomycin (1% v/v) was added to well with the scaffold before the DRG were placed onto the scaffold and at a volume so that the DRG were not completely submerged in the media (~500 uL). For the untethered SPIONs group, 500 uL of 10 μg/mL SPIONs in neuron growth media was added to wells with control PLLA scaffolds before the DRG were seeded. A total of 2-3 DRG were placed on one scaffold to ensure that extending neurites did not overlap with neurites from other DRG on the scaffold for analysis purposes. The scaffolds were then placed in a cell culture incubator at 37°C and 5% CO_2. The DRG were allowed to adhere to the scaffolds for 24h before the scaffolds were placed into the magnetic fields described above and with fresh neuron growth media. The DRG were incubated for an additional 48 h in the magnetic fields before fixing.

2.11. Cell Immunocytochemistry and Confocal Imaging

Immunocytochemistry was used to assess neurite outgrowth and Schwann cell migration from DRG cultured on the different fiber types and in the different magnetic fields. DRG were fixed in 4% paraformaldehyde for 15 min, then washed three times with phosphate buffered saline (PBS). After fixing, the side of the scaffold closest to the magnet was marked so that this

information was considered while imaging and comparing neurite outgrowth between groups. To assess neurite outgrowth in the different conditions, the DRG were stained for neurofilament. First, the DRG were blocked in 5% bovine serum albumin (BSA) and 0.01% Triton X in PBS for 1 h at room temperature. Then the primary antibody solution was added, consisting of a 1:500 dilution of RT97 in 5% BSA and 0.1% Tween 20 in PBS. The scaffolds were then incubated at 4°C overnight. Next, the scaffolds were washed three times with PBS to remove any unbound primary antibody and the secondary antibody solution was added, consisting of a 1:1000 dilution of Alexaflour 488 donkey-anti-mouse in 5% BSA and 0.1% Tween 20. The scaffolds were incubated in secondary antibody solution for 1 h at room temperature protected from light. A solution of DAPI diluted 1:1000 in PBS was then added to scaffolds and incubated for 10 min at room temperature protected from light to label all nuclei. The scaffolds were then washed twice with PBS to remove unbound secondary antibody and DAPI, then stored in PBS at 4°C until they were imaged.

An Olympus IX-81 Confocal Microscope (Melville, NY) equipped with Metamorph Premier 7.7.3.0 (Sunnyvale, CA) was used to acquire Z-series stacked images of the DRG at 4X magnification for analysis. Green fluorescent protein (GFP; $\lambda_{ex}488/ \lambda_{em}510$) and DAPI ($\lambda_{ex}358/ \lambda_{ex}461$) fluorescence channels were used to acquire images of neurofilament and nuclei, respectively. Multiple images of the DRG and extending neurites were taken with overlap between the different views to ensure that images could be stitched together to view the entire DRG with its extending neurites. Images were taken such that the side of the scaffold closest to the magnet was on the right side of the image.

2.12. Neurite Outgrowth Analysis of Whole DRG

To analyze neurite outgrowth from the DRG, z-series stacks in the GFP channel were first collapsed by creating the maximum intensity projection using ImageJ software (NIH) and subtracting background from each image (rolling=50). All the neurofilament images for one DRG were then stitched together using Adobe Photoshop CS2. The five longest neurites on one side of the DRG were measured by drawing a line in ImageJ from the tip of the neurite to the edge of the DRG body and recording its length. One side of the DRG was considered a separate replicate from the opposite side and at least n=12 average longest neurite measurements were assessed per group. An in-house written MATLAB code was then used to assess the area of the extending neurites in binned regions at different distances from the DRG body. The center point and dimensions of each DRG were first measured using the oval tool in ImageJ. Then with the MATLAB code, the DRG images were converted to a binary image with a constant threshold for all images unless significant background was included, and then the threshold was increased to only include the neurofilament signal. The DRG body measurements were then inputted for the specific DRG being analyzed, and the DRG body was then excluded so that only the area of the extending neurites was analyzed. The area of the neurites was recorded for increasing distance from the DRG body in 500 um bins with a maximum measurement of 5.5-6.0 mm away from the DRG (the maximum distance found from the longest neurite analysis). The code recorded the area in these bins on all sides of the DRG, on the right side of the DRG (corresponding to the side closest to the magnet), and on the left side of the DRG (the side farther from the magnet).

2.13. Analysis of Schwann Cell Migration from Whole DRG

To analyze cell migration from the DRG, z-series stacks in the DAPI channel were first collapsed by creating the maximum intensity projection using ImageJ software (NIH) and subtracting background from each image (rolling=50). All the DAPI images for one DRG were

then stitched together using Adobe Photoshop CS2. The same in-house written MATLAB code used for analyzing neurite area was then used to assess the area of DAPI signal and estimate the number of cells in binned regions at different distances from the DRG body. The area of the nuclei was recorded for increasing distance from the DRG body in 500 um bins with a maximum measurement of 5.5-6.0 mm away from the DRG to be consistent with the neurite area analysis. The code recorded the area in these bins on all sides of the DRG, on the right side of the DRG (corresponding to the side closest to the magnet), and on the left side of the DRG (the side farther from the magnet). To estimate the number of cells in a bin, the average number of pixels in a single stained nucleus was calculated using ImageJ. A total of 100 nuclei were measured from images of DRG isolated from three different animals.

2.14. Statistical Analysis

Statistical analysis was performed using Minitab 19. First, data normality was assessed using a Ryan-Joiner Test. The data from each group for a given experiment was then tested for equal variances, either assuming normality or not based on the normality test. If the test compared only two groups (fiber diameter, density, alignment, and contact angle), a two-sample t-test was used if the data were normally distributed and Mood's Median test was used for non-normally distributed data. For comparisons of more than two groups, a one-way ANOVA and Tukey's post hoc test was used for normally distributed data with equal variances, while Welch's ANOVA and Games-Howell post hoc test was used for non-normally distributed data and/or if groups did not have equal variances. For neurite outgrowth and Schwann cell migration data, statistical analyses were conducted between fiber types (control, SPION-grafted, untethered SPIONs) for a given magnetic field condition as well as between magnetic field conditions (none, static, alternating, linearly moving) for a given fiber type.

3. Results
3.1. Characterization of Electrospun Fiber Scaffolds

In this study, we grafted SPIONs to the surface of aligned PLLA fibers and assessed their ability to affect neurite outgrowth in combination with different types of magnetic fields. We first used SEM to confirm successful SPION grafting and then characterize the morphology of control PLLA fibers (Figure 2A) and SPION-grafted PLLA fibers (Figure 2B). Fiber diameter (Figure 2C) was the same for control (2.02 ± 0.20 µm) and SPION-grafted (2.15 ± 0.27 µm) fibers. Fiber density on the coverslip (Figure 2D) was also found to be the same for control (361.4 ± 110.7 fibers/mm) and SPION-grafted (463.6 ± 98.6 fibers/mm) fibers. FFT analysis was used to generate greyscale pixel images (Figure 2E) that reflect the degree of fiber alignment. These images were then analyzed for pixel intensity in radial sums in 1° increments. These data were normalized to the maximum pixel intensity and plotted for ± 50° from the maximum intensity, which corresponds to the direction that most of the fibers are oriented on the scaffold. The area under the curve plotted in Figure 2F corresponds to the degree of fiber alignment; a larger area indicates that the fibers are less aligned. SPION-grafted fibers (area = 27.29 ± 2.38 arbitrary units) were significantly less aligned (p=0.001) than control fibers (area = 17.81 ± 2.46 arbitrary units), but the FFT curves are a similar shape (Figure 2F). Because surface hydrophilicity can affect cell adhesion and neurite extension [29], static water contact angle (Figure 2G) was measured to determine differences in surface hydrophilicity between control PLLA and SPION-grafted PLLA fibers. The contact angle was not statistically different between control (120.7 ± 10.0°) and SPION-grafted (123.8 ± 8.5°) fibers. These measurements indicate that the grafted SPIONs do not increase the hydrophobicity of PLLA fibers.
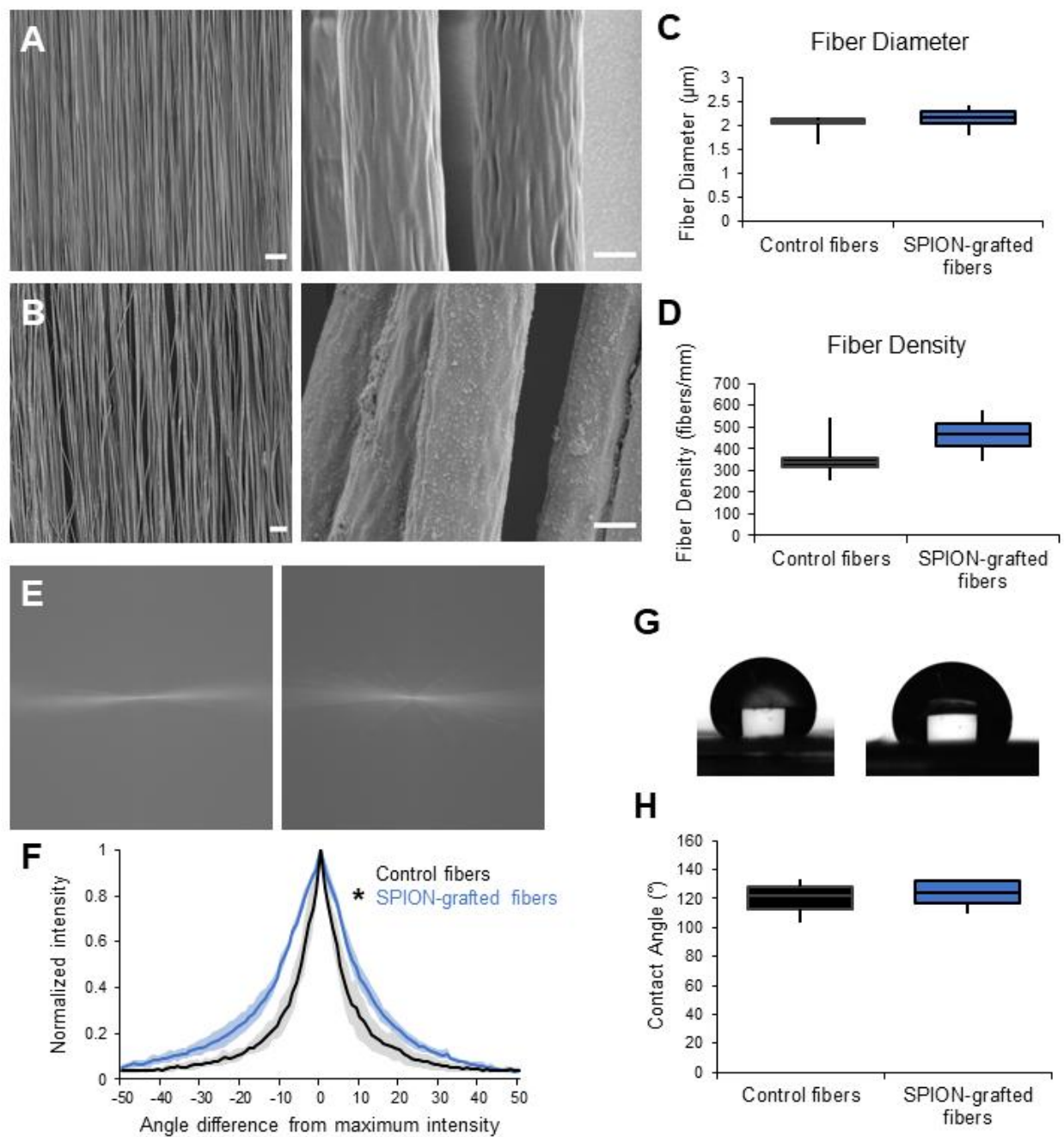
Figure 2: Electrospun fiber characterization. Low (left, scale bar = 50 µm) and high (right, scale bar = 1 µm) magnification scanning electron micrographs of control PLLA fibers (A) and SPION-grafted PLLA fibers (B). Boxplots show quantification of fiber diameter (C) and fiber density (D). Sample FFT output images for control (left) and SPION-grafted (right) fibers are shown in (E). Fiber alignment was characterized from FFT images analyzed for pixel intensity and normalized data is plotted in (F). Statistical significance comparing area under the curve was assessed using a two-sample t-test (*$p < 0.05$). Shaded region around the solid line indicates ± standard deviation. Sample images of water droplets on control (left) and SPION-grafted (right) fibers used to analyze static water contact angle are shown in (G). The boxplot shows the contact angle measurements for control and SPION-grafted fibers (H).

3.2. Characterization of Grafted SPIONs

To characterize the nanoscale features that cells experience when cultured on the SPION-grafted fibers, we analyzed the density of grafted SPIONs using high magnification SEM images (Figure 3A). The average grafting density was 38.5 ± 18.3 SPIONs/µm² across all fabrication batches (Figure 3C). A 1 µm² box is outlined in red on a fiber in Figure 3A for reference. Due to the inherent instability of individual SPIONs [30], some aggregation did occur during the grafting process. Larger SPION aggregates were mostly removed in a sonication step after the grafting procedure, but smaller aggregates remained on the scaffold (Figure 3B yellow arrow). Because neurite outgrowth can be affected by fiber surface topography [28], we further characterized the microscale features of the SPION-grafted fiber scaffolds by analyzing the average aggregate density and average aggregate size. A cluster of SPIONs was considered an aggregate if the cluster area was greater than 0.05 µm². The average number of aggregates was 5.7 ± 4.4 per 100 µm² (Figure 3D) and the average size of the aggregates was 0.506 ± 0.544 µm² (Figure 3E). A 100 µm² box is outlined in red in Figure 3B and the yellow arrow points at an 0.4 µm² SPION aggregate for reference.
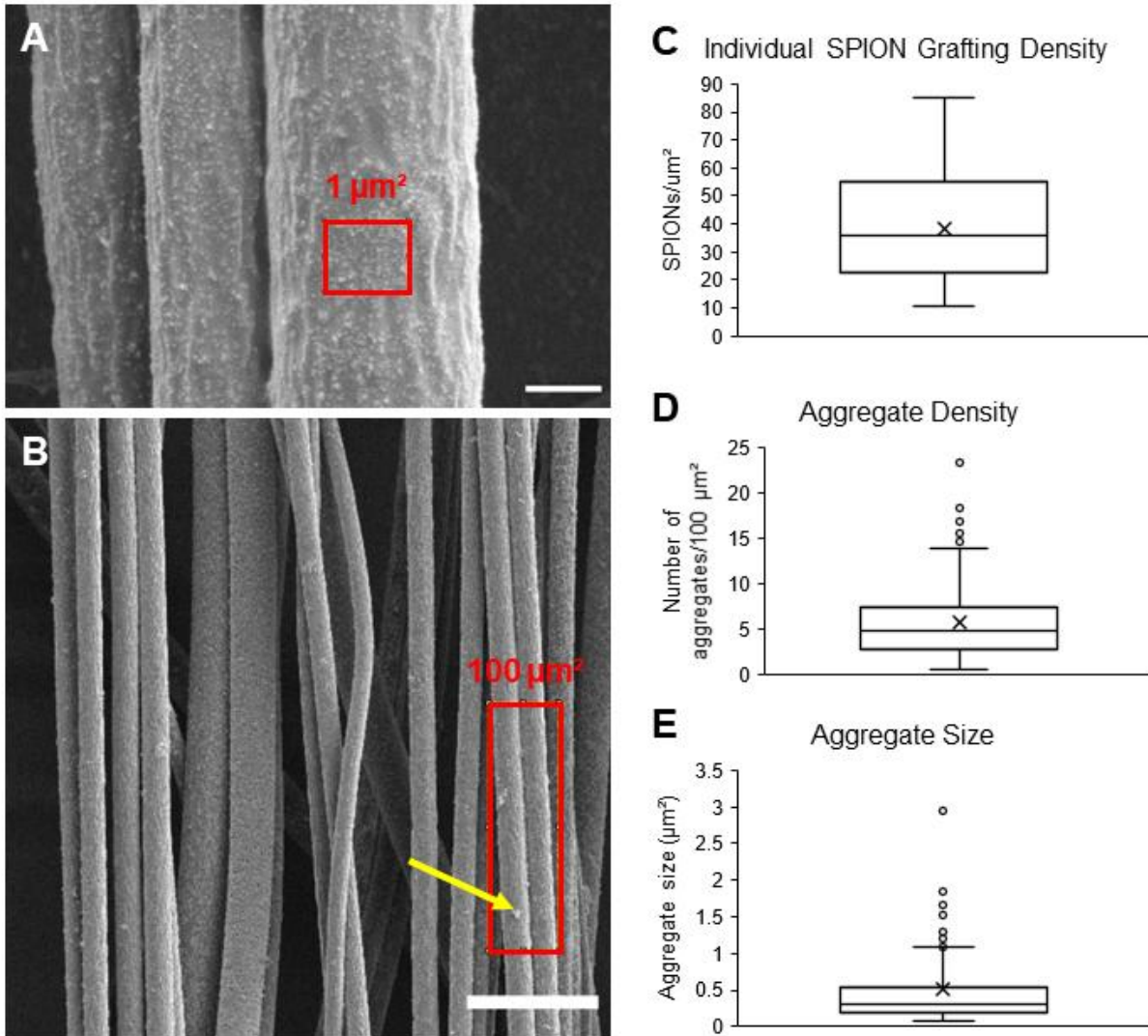
Figure 3: Characterization of grafted SPIONs on PLLA fibers. A) High magnification SEM of SPION-grafted fibers with a red box indicating a 1 square micron area (scale bar = 1 µm). B) Lower magnification SEM of SPION-grafted fibers with a red box indicating a 100 square micron area (scale bar = 10 µm). Yellow arrow points to an aggregate of SPIONs. The boxplots show the quantification of the SPION grafting density in number of SPIONs per 1 µm² (C), SPION aggregate density in number of aggregates per 100 µm² (D), and the aggregate size in µm² (E).

3.3. Magnetic Field Simulations

To determine how different types of magnetic fields affect neurite outgrowth, a static, alternating, and linearly moving magnetic field were created using permanent neodymium cylinder magnets (1.43 T). For each magnetic field condition, the magnet pole was initially centered 10 mm from one side of the scaffold. To characterize the magnetic field at different areas on the scaffold, Quickfield software was used to simulate the magnetic field flux density as a function of distance from the magnet. Figure 4A shows a color map depicting the magnitude of the magnetic flux density in mT and the arrows depicting the vector direction of the field. The magnet is outlined on the left and the square scaffold is outlined on the right, with the three points of interest are labeled: the edge of the scaffold closest to the magnet, the center of the scaffold, and the edge of the scaffold farthest from the magnet. In the static magnetic field condition and at the initial positions for the alternating and linearly moving magnetic fields, the flux density is 115 mT at the edge of the scaffold closest to the magnet, 50 mT at the center of the scaffold, and 26 mT at the edge of the scaffold farthest from the magnet (Figure 4B). In the alternating field condition, the magnet rotates 360° every 1 s, so the flux density oscillates twice from 115–150 mT on the edge of the scaffold closest to the magnet, from 50–64 mT at the center of the scaffold, and from 26–41 mT on the edge of the scaffold farthest from the magnet (Figure 4C). The flux density increases because the center point of the magnet is conserved while it rotates, so the edges of the cylinder become closer to the scaffold and therefore increase the flux density. In the linearly moving magnetic field condition, the magnet is moved 10 mm away from the scaffold and back again at 2 mm/s. The simulation showed that the flux density decreases from 115 to 40 mT at the edge of the scaffold closest to the magnet, from 50 to 22 mT at the

center of the scaffold, and from 26 to 13 mT at the edge of the scaffold farthest from the magnet over the course of 5 s as the magnet moves away from the scaffold.
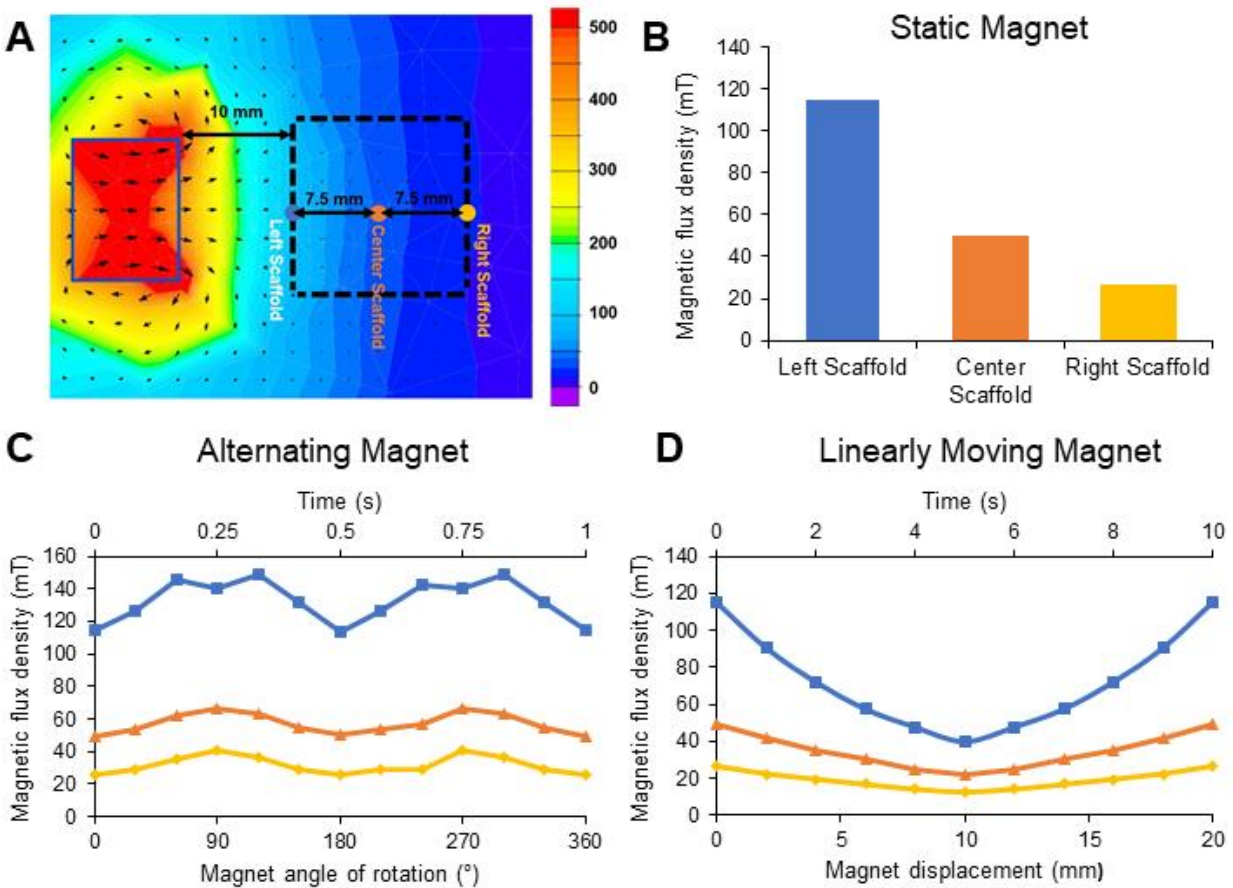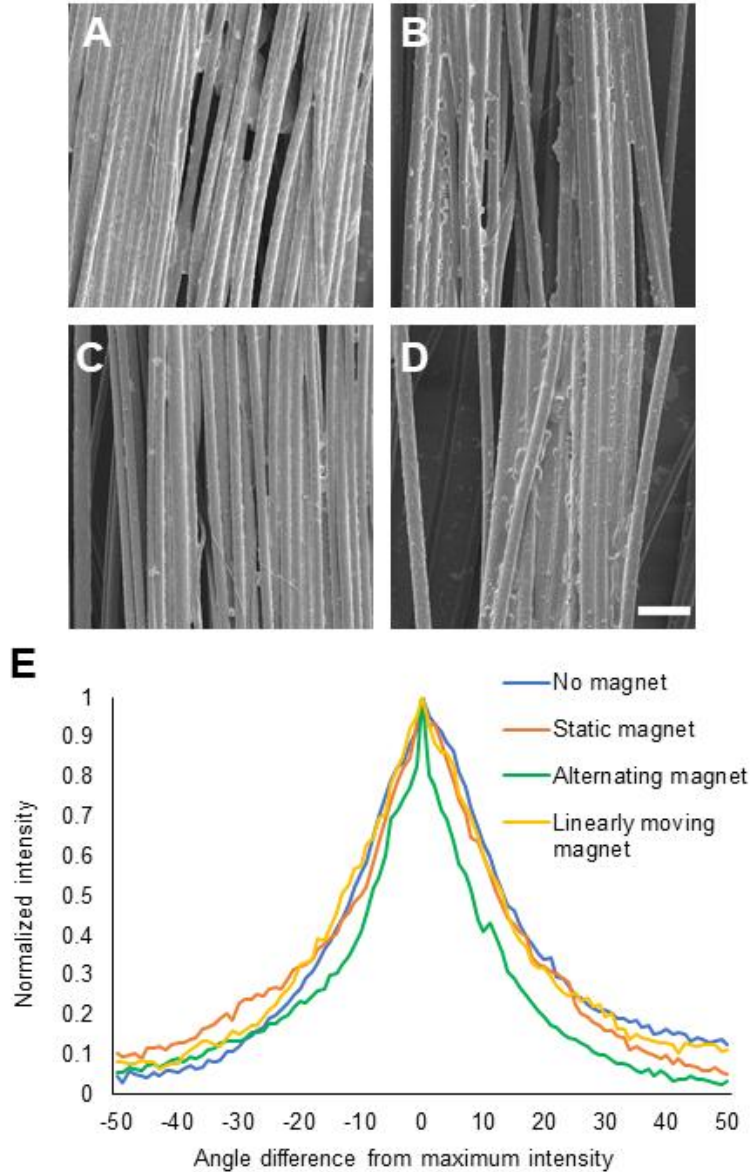
Figure 4: Magnetic field simulations. A) Color map indicating magnetic field flux density (scale bar in mT). The scaffold is outlined with a black dotted line and the points on the scaffold correspond to the graphed flux densities. At time 0 s, the left side of the scaffold is 10 mm from the magnet. B) Graph showing the magnetic flux density at the three points on the scaffold in the static magnetic field condition (blue squares for left scaffold, orange triangles for center scaffold, and yellow diamonds for right scaffold). C) Graph showing the magnetic flux density over time and as the magnet rotates in the alternating magnetic field condition. D) Graph showing the magnetic flux density over time as the magnet moves away from and toward the scaffold in the linearly moving magnetic field condition.

3.4. Analysis of SPION-Grafted Scaffolds After Incubation in Magnetic Fields

The magnetic susceptibility of the SPION-grafted fibers was previously demonstrated [24], but the impact of prolonged exposure to an external magnetic field on SPION-grafted fiber scaffold morphology was not characterized. Therefore, we incubated the scaffolds in water at physiological conditions (37°C, 5% CO_2) in the three types of magnetic fields for 2 days to mimic the exposure used for cell experiments. Comparing the SEM images of scaffolds incubated in no magnetic field (Figure 5A), the static magnetic field (Figure 5B), the alternating magnetic field (Figure 5C), and the linearly moving magnetic field (Figure 5D), there were no major differences in fiber morphology. FFT analysis was used to quantify changes in fiber alignment; no statistical differences were seen between groups (Figure 5E).

Figure 5: Analysis of SPION-grafted fibers after incubation in magnetic fields. SEM images of SPION-grafted fibers after a 48-h incubation in water with either A) no magnetic field, B) a static magnetic field, C) an alternating magnetic field, or D) a linearly moving magnetic field. E) FFT analysis of SEM images to characterize fiber alignment.

3.5. DRG Neurite Outgrowth Analysis

To examine the effects of different types of magnetic fields on neurite outgrowth from neurons cultured on electrospun fibers and investigate the effect of SPION-grafted fibers on

neurite outgrowth, neonatal rat DRG were cultured on fiber scaffolds for one day to allow the DRG to adhere and then cultured for an additional two days in the different types of magnetic fields. In addition to culturing DRG on control PLLA fibers and SPION-grafted PLLA fibers, DRG were also cultured on control PLLA fibers in the presence of 10 μg/mL SPIONs dispersed in the culture media ("untethered SPIONs"). After the three-day culture period, the DRG were then fixed and stained for neurofilament and DAPI to assess neurite outgrowth and Schwann cell migration from the DRG, respectively. Neurite outgrowth was characterized by analyzing both the average longest neurite and total neurite area coverage. There were no significant differences in the average longest neurite from DRG between each of the fiber conditions when no magnetic field or when the linearly moving magnetic field was present (Figure 6A). However, neurites extended significantly farther on SPION-grafted fibers than when incubated with untethered SPIONs in both the static (p=0.016) and alternating magnetic fields (p=0.009). Additionally, DRG cultured on control fibers also extended longer neurites than DRG cultured with untethered SPIONs in the alternating magnetic field (p=0.000). Looking at how different magnetic field types affect neurite outgrowth on control PLLA fibers, DRG had significantly longer neurites after culture in the alternating and linearly moving magnetic fields compared to a static magnetic field (p=0.000).

Because the magnetic field flux density varies by more than 100 mT across the scaffold, we also compared neurite outgrowth on the side of the DRG closest to the magnet to the side farther from the magnet by plotting the ratio of the two (Figure 6B). A ratio greater than 1 indicates more neurite area on the side of the DRG closest to the magnet. There was significantly more neurite area on the side of the DRG closest to the magnet when DRG were cultured on SPION-grafted fibers and incubated in the static (p=0.037) or alternating magnetic field

(p=0.038) compared to the linearly moving magnetic field, where the area was approximately equal on both sides of the DRG. The ratio trends much higher than 1 in the alternating magnetic field for DRG cultured on both SPION-grafted fibers (ratio = 1.92 ± 1.61) and DRG incubated with untethered SPIONs (ratio = 1.91 ± 1.35). Additionally, the ratio of neurite area from DRG cultured on control PLLA fibers in the static magnetic field (ratio = 1.58 ± 0.70) trended higher than DRG cultured on control fibers in the linearly moving magnetic field (p=0.064).

Neurite area was further analyzed in bins of 2 mm moving away from the DRG body. There were no significant changes in area between the fiber types when no magnetic field or the static or linearly moving magnetic field was present (Supporting Information Figures XX). However, DRG incubated with untethered SPIONs in the alternating magnetic field had significantly less neurite area in many of the binned regions (Figure 6D). Representative confocal images of DRG cultured on control, SPION-grafted, and untethered SPION scaffolds in the alternating magnetic field show the trend for greater neurite area on the side of the DRG closest to the magnet (indicated by the red arrow) for the SPION-grafted and untethered SPION scaffolds (Figure 6C). These images also highlight the significantly decreased neurite length from the DRG cultured with the untethered SPIONs compared to the DRG cultured on control and SPION-grafted fibers.
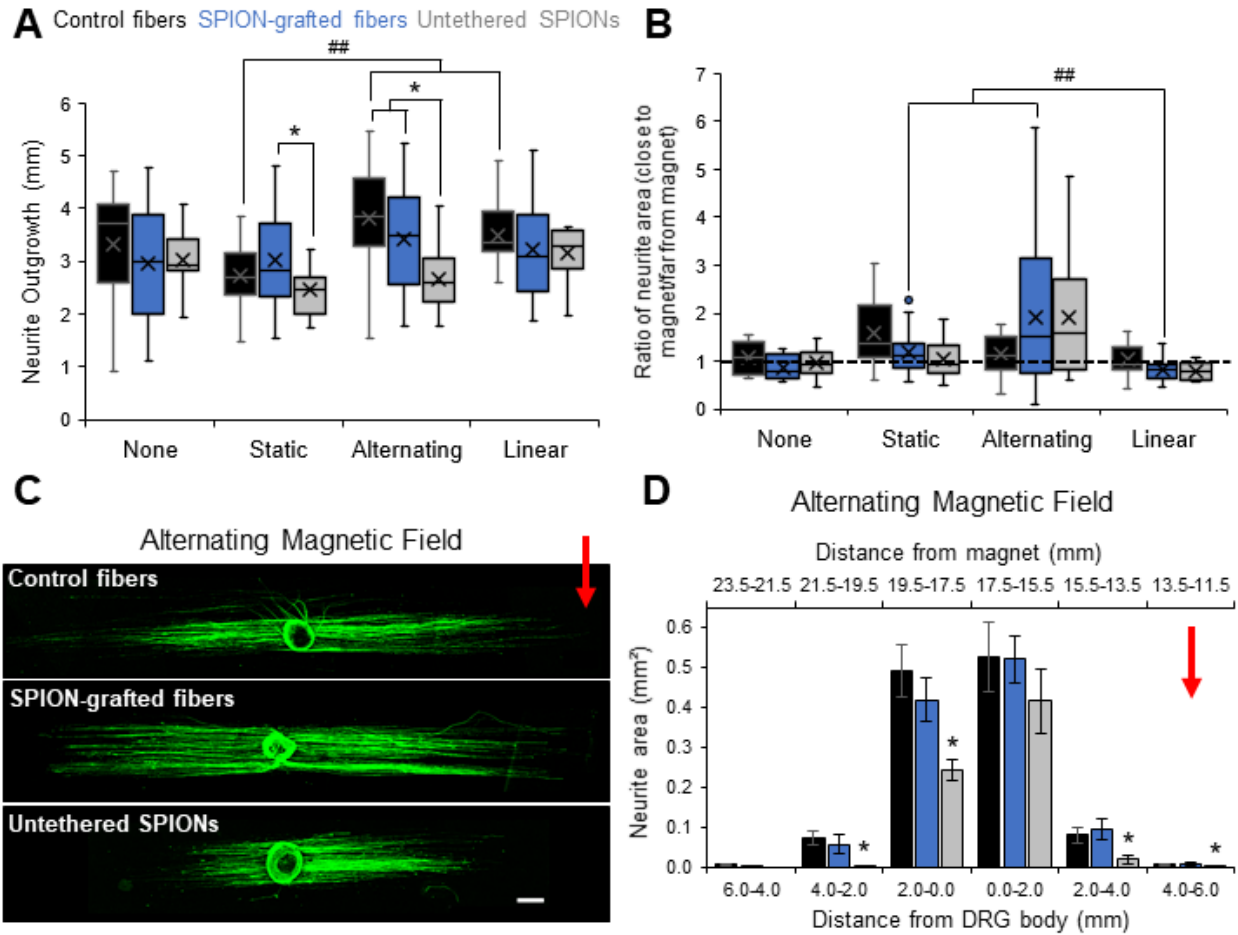
Figure 6: Analysis of neurite outgrowth from DRG. A) Summary boxplot displays the average longest neurite for each fiber type in each magnetic field condition. Statistical significance between fiber type was assessed using Welch's ANOVA and Games-Howell post hoc test (*p < 0.05). Statistical significance between magnetic field condition for one fiber type was assessed using Welch's ANOVA and Games-Howell post hoc test (##p < 0.001). B) Summary boxplot displays the ratio of total neurite area on the side of the DRG closest to the magnet to total neurite area on the side of the DRG farther from the magnet. Statistical significance between magnetic field condition for one fiber type was assessed using Welch's ANOVA and Games-Howell post hoc test (##p < 0.001). C) Representative confocal images of DRG stained for neurofilament (green) on control fibers, SPION-grafted fibers, and control fibers incubated with untethered SPIONs in the alternating magnetic field condition (scale bar = 500 µm). The red arrow points to the side of the DRG closest to the alternating magnet. D) Summary graph of neurite area for each fiber type in the alternating magnetic field condition in binned regions from the DRG body. Error bars indicate ± standard error of the mean. Statistical significance between fiber type at a given bin was assessed using Welch's ANOVA and Games-Howell post hoc test (*p < 0.05). The red arrow points to the side of the DRG closest to the alternating magnet.

3.6. Schwann Cell Migration from DRG Body

The DRG explants contain neurons as well as Schwann cells. Individual cells will migrate away from the DRG body along the electrospun fibers, primarily consisting of Schwann cells. This migration behavior can be affected by the fiber properties [31,32]. To characterize differences in migration patterns from the DRG on SPION-grafted fibers and in the different magnetic fields, images of DAPI-stained nuclei were analyzed for the number of cells in 2 mm binned regions from the DRG body. There were no significant differences in the number of nuclei that migrated 0–2 mm away from the DRG (Supporting Information Figure XX), but there were some differences in the number of nuclei in the 2–4 mm region (Figure 7B). Though only statistically significant in the static and linearly moving magnetic field, the general trend is that the presence of any type of magnetic field results in less cells that migrated into the 2–4 mm region if the DRG were incubated with untethered SPIONs compared to DRG cultured on control or SPION-grafted fibers. Interestingly, there was a significant increase in the number of cells that migrated 2–4 mm away from the DRG body on control fibers when incubated in the linearly moving magnetic field compared to the no magnet control. The migration patterns on the different fiber types in the alternating magnetic field mimic the patterns of neurite outgrowth – farther migration and neurite extension on the control and SPION-grafted fibers compared to DRG cultured on control fibers with untethered SPIONs (Figure 7A). There were no differences in the number of Schwann cells that migrated on the side of the DRG closer to the magnet (indicated by the red arrow in Figure 7) compared to the side of the DRG farther from the magnet.
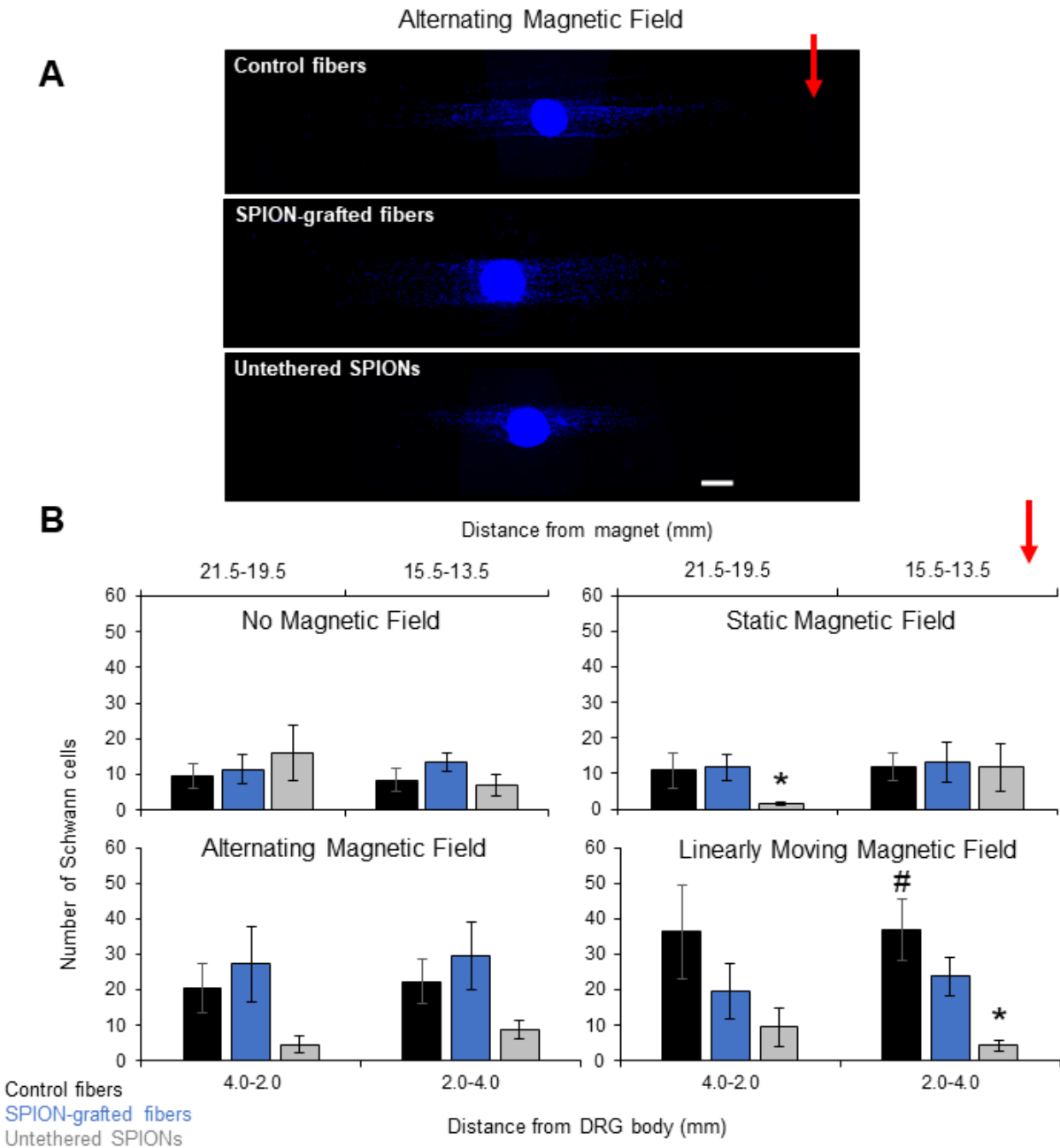
Figure 7: Analysis of Schwann cell migration from DRG. A) Representative confocal images of DAPI-stained DRG cultured on the different fiber types in the alternating magnetic field condition (scale bar = 500 µm). The red arrow points to the side of the DRG closest to the alternating magnet. B) Summary graph of Schwann cell number for each fiber type and each magnetic field condition in the 2-4 mm region from the DRG body. Error bars indicate ± standard error of the mean. Statistical significance between fiber type at a given bin was assessed using Welch's ANOVA and Games-Howell post hoc test (*$p < 0.05$). Statistical significance between magnetic field condition for one fiber type was assessed using Welch's ANOVA and Games-Howell post hoc test (#$p < 0.05$). The red arrow points to the side of the DRG closest to the alternating magnet.

4. Discussion

In this study, we investigated the potential of SPION-grafted aligned PLLA electrospun fibers in combination with different types of magnetic fields to promote axonal regeneration. To do this, we cultured neonatal rat DRG on control PLLA fibers, SPION-grafted PLLA fibers, and control PLLA fibers with untethered SPIONs dispersed in the culture media and incubated the scaffolds in either no magnetic field, a static magnetic field, an alternating magnetic field, or a linearly moving magnetic field. We then assessed neurite outgrowth and Schwann cell migration from the DRG in each of these conditions.

To our knowledge, no previous study has examined the effects of magnetic field stimulation on neurite outgrowth from neurons cultured on electrospun fibers, so we first asked whether different types of magnetic fields affect neurite outgrowth on aligned PLLA fibers. We found that neurite length significantly increased on aligned PLLA fiber scaffolds in both types of dynamic magnetic fields tested (alternating and linearly moving) compared to a static magnetic field, but the total area covered by extending neurites was not affected by magnetic field stimulation on control PLLA fibers. Pulsed magnetic fields have been shown to increase neurite and axonal outgrowth from both neuronal cell lines and primary neurons when cultured on routine 2D tissue culture surfaces [6–8,33,34]. However, the effects are dependent on the strength of the magnetic field, the pulse frequency, and the length of the pulse [8,34]. The magnetic fields used in these studies are in the mT range, similar to the magnetic fields used in this study. One study by Kim et al. showed that PC12 cells exposed to a 12-mT static magnetic field extended more neurites and longer neurites perpendicular to the direction of the applied magnetic field. Further, neurites that extended in the direction of the magnetic field appeared to be dystrophic, beaded, or thickened [35]. This could explain the trended decrease in neurite

length from DRG cultured on control PLLA fibers in the static magnetic field (Figure 6A), because the aligned fibers were oriented in the direction of the magnetic field. Osteoblasts cultured on aligned fiber scaffolds will actually start to orient in the direction of a 10-mT static magnetic field, despite the topography of the aligned fibers guiding orientation perpendicular to the field [36]. In this study, extending neurites did not appear to deviate from the fiber orientation when incubated in the static magnetic field, but neurite length was significantly decreased compared to the alternating and linearly moving magnetic field (Figure 6A).

We also explored the combination of magnetic field stimulation with magnetic composite fibers on neurite outgrowth. There have been several studies that utilize SPIONs as magnetic actuators to guide cellular migration or, with neurons specifically, guide neurite outgrowth [10]. Therefore, we also incubated DRG cultured on control PLLA fibers with untethered SPIONs to examine differences in how the neurons interact with SPIONs that are grafted to a surface compared to free, dispersed SPIONs within different magnetic fields. DRG incubated with untethered SPIONs had significantly shorter neurite lengths in the static and alternating magnetic fields than DRG cultured on SPION-grafted fibers (Figure 6A), as well as significantly less neurite area in the alternating magnetic field compared to DRG cultured on SPION-grafted fibers (Figure 6D). PC12 cells incubated with SPIONs preferentially extended neurites in the direction of a static magnetic field [11,13]. Further, an alternating magnetic field increased neurite outgrowth from PC12 cells incubated with SPIONs more so than a static magnetic field [15]. We observed increases in both neurite length and neurite area from DRG cultured on SPION-grafted fibers compared to untethered SPIONs in the alternating magnetic field. Neurite outgrowth was not affected by the untethered SPIONs when there was no magnetic field present, indicating that it is the combination of magnetic field stimulation with untethered SPIONs that hindered neurite

34

outgrowth. Interestingly, there was significantly more neurite area on the side of the DRG closest to the magnet in the alternating field on SPION-grafted fibers and a similar trend for DRG incubated with untethered SPIONs in the alternating field. Looking specifically at neurite area from DRG incubated with untethered SPIONs in the different binned regions (Figure 6D), the area is the same as control and SPION-grafted fibers 0-2mm on the side of the DRG closer to the magnet, but then trails off quickly in both directions. It may be that there is a "sweet spot" for the untethered SPIONs to improve neurite outgrowth, where the magnetic field strength is not too high where the forces from the SPIONs are detrimental to neurite extension and not too low that there is no added force from the untethered SPIONs.

In addition to examining changes in neurite outgrowth, we also analyzed Schwann cell migration from the DRG on the different fiber scaffolds in the different magnetic fields. Significantly less Schwann cells migrated 2-4 mm on the side of the DRG farther from the magnet when incubated with untethered SPIONs compared to DRG cultured on control or SPION-grafted fibers (Figure 7B). Several studies have shown that Schwann cells incubated with SPIONs will migrate toward a magnetic field [37–39], so this could explain why less Schwann cells migrated farther away from the magnet when incubated with untethered SPIONs on control fibers. Interestingly, significantly more Schwann cells migrated 2-4 mm away from the DRG on control fibers in the linearly moving magnetic field compared to when no magnetic field was present, mimicking the trend of neurite length.

It can become difficult to compare between studies when there are many different parameters that can affect the result, as is the case with magnetic field stimulation on cells. We directly compare a static, alternating, and linearly moving magnetic field and show that an alternating magnetic field increases neurite length from rat DRG on aligned control and SPION-

grafted PLLA fibers compared to a static magnetic field. Additionally, we show that both neurite length and area coverage are increased on SPION-grafted PLLA fibers compared to cells cultured on control PLLA fibers with untethered, dispersed SPIONs added to the culture media. These findings show the potential of combining magnetic field stimulation with magnetic fiber composites for neural regeneration, but more work is needed to further optimize these different parameters for neuro-specific applications.

Acknowledgements

Disclosure of Interest

All contributing authors have no conflicts of interest to disclose.

References

[1] N.J. Schaub, C.D. Johnson, B. Cooper, R.J. Gilbert, Electrospun Fibers for Spinal Cord Injury Research and Regeneration, J Neurotrauma. 33 (2016) 1405–1415. https://doi.org/10.1089/neu.2015.4165.

[2] A. Hurtado, J.M. Cregg, H.B. Wang, D.F. Wendell, M. Oudega, R.J. Gilbert, J.W. McDonald, Robust CNS regeneration after complete spinal cord transection using aligned poly-l-lactic acid microfibers, Biomaterials. 32 (2011) 6068–6079. https://doi.org/10.1016/j.biomaterials.2011.05.006.

[3] C. Xue, H. Zhu, D. Tan, H. Ren, X. Gu, Y. Zhao, P. Zhang, Z. Sun, Y. Yang, J. Gu, Y. Gu, X. Gu, Electrospun silk fibroin-based neural scaffold for bridging a long sciatic nerve gap in dogs, J Tissue Eng Regen Med. 12 (2018) e1143–e1153. https://doi.org/10.1002/term.2449.

[4] J.I. Kim, C.S. Kim, C.H. Park, Harnessing Nanotopography of Electrospun Nanofibrous Nerve Guide Conduits (NGCs) for Neural Tissue Engineering, Adv. Exp. Med. Biol. 1078 (2018) 395–408. https://doi.org/10.1007/978-981-13-0950-2_20.

[5] A.R. D'Amato, A.M. Ziemba, C.D.L. Johnson, R.J. Gilbert, 18 - Advances in the use of electrospun fibers for the central nervous system, in: V. Guarino, L. Ambrosio (Eds.), Electrofluidodynamic Technologies (EFDTs) for Biomaterials and Medical Devices, Woodhead Publishing, 2018: pp. 377–398. https://doi.org/10.1016/B978-0-08-101745-6.00018-9.

[6] R. Lekhraj, D.E. Cynamon, S.E. DeLuca, E.S. Taub, A.A. Pilla, D. Casper, Pulsed electromagnetic fields potentiate neurite outgrowth in the dopaminergic MN9D cell line, Journal of Neuroscience Research. 92 (2014) 761–771. https://doi.org/10.1002/jnr.23361.

[7] B. Greenebaum, C.H. Sutton, M.S. Vadula, J.H. Battocletti, T. Swiontek, J. DeKeyser, B.F. Sisken, Effects of pulsed magnetic fields on neurite outgrowth from chick embryo dorsal root ganglia, Bioelectromagnetics. 17 (1996) 293–302. https://doi.org/10.1002/(SICI)1521-186X(1996)17:4<293::AID-BEM5>3.0.CO;2-Z.

[8] Y. Zhang, J. Ding, W. Duan, W. Fan, Influence of pulsed electromagnetic field with different pulse duty cycles on neurite outgrowth in PC12 rat pheochromocytoma cells, Bioelectromagnetics. 26 (2005) 406–411. https://doi.org/10.1002/bem.20116.

[9] M.Y. Macias, J.H. Battocletti, C.H. Sutton, F.A. Pintar, D.J. Maiman, Directed and enhanced neurite growth with pulsed magnetic field stimulation, Bioelectromagnetics. 21 (2000) 272–286. https://doi.org/10.1002/(SICI)1521-186X(200005)21:4<272::AID-BEM4>3.0.CO;2-5.

[10] J.L. Funnell, B. Balouch, R.J. Gilbert, Magnetic Composite Biomaterials for Neural Regeneration, Front. Bioeng. Biotechnol. 7 (2019). https://doi.org/10.3389/fbioe.2019.00179.

[11] C. Riggio, M.P. Calatayud, M. Giannaccini, B. Sanz, T.E. Torres, R. Fernández-Pacheco, A. Ripoli, M.R. Ibarra, L. Dente, A. Cuschieri, G.F. Goya, V. Raffa, The orientation of the neuronal growth process can be directed via magnetic nanoparticles under an applied magnetic field, Nanomedicine: Nanotechnology, Biology and Medicine. 10 (2014) 1549–1558. https://doi.org/10.1016/j.nano.2013.12.008.

[12] J.M. Zuidema, C. Provenza, T. Caliendo, S. Dutz, R.J. Gilbert, Magnetic NGF-Releasing PLLA/Iron Oxide Nanoparticles Direct Extending Neurites and Preferentially Guide Neurites along Aligned Electrospun Microfibers, ACS Chem. Neurosci. 6 (2015) 1781–1788. https://doi.org/10.1021/acschemneuro.5b00189.

[13] M. Marcus, M. Karni, K. Baranes, I. Levy, N. Alon, S. Margel, O. Shefi, Iron oxide nanoparticles for neuronal cell applications: uptake study and magnetic manipulations, J Nanobiotechnology. 14 (2016). https://doi.org/10.1186/s12951-016-0190-0.

[14] Y. Jin, J. Lee, E. Chung, K. Yang, J. Kim, J. Kim, J.S. Lee, A.-N. Cho, T. Oh, J.-H. Lee, S.-W. Cho, J. Cheon, Magnetic Control of Axon Navigation in Reprogrammed Neurons, Nano Lett. 19 (2019) 6517–6523. https://doi.org/10.1021/acs.nanolett.9b02756.

[15] M. Yuan, Y. Wang, Y.-X. Qin, Promoting neuroregeneration by applying dynamic magnetic fields to a novel nanomedicine: Superparamagnetic iron oxide (SPIO)-gold nanoparticles bounded with nerve growth factor (NGF), Nanomedicine: Nanotechnology, Biology and Medicine. 14 (2018) 1337–1347. https://doi.org/10.1016/j.nano.2018.03.004.

[16] H.-J. Lee, S.J. Lee, S. Uthaman, R.G. Thomas, H. Hyun, Y.Y. Jeong, C.-S. Cho, I.-K. Park, Biomedical Applications of Magnetically Functionalized Organic/Inorganic Hybrid Nanofibers, Int J Mol Sci. 16 (2015) 13661–13677. https://doi.org/10.3390/ijms160613661.

[17] T.-C. Lin, F.-H. Lin, J.-C. Lin, In vitro feasibility study of the use of a magnetic electrospun chitosan nanofiber composite for hyperthermia treatment of tumor cells, Acta Biomater. 8 (2012) 2704–2711. https://doi.org/10.1016/j.actbio.2012.03.045.

[18] R.J.R. Matos, C.I.P. Chaparro, J.C. Silva, M.A. Valente, J.P. Borges, P.I.P. Soares, Electrospun composite cellulose acetate/iron oxide nanoparticles non-woven membranes for magnetic hyperthermia applications, Carbohydr Polym. 198 (2018) 9–16. https://doi.org/10.1016/j.carbpol.2018.06.048.

[19] B. Wang, H. Zheng, M.-W. Chang, Z. Ahmad, J.-S. Li, Hollow polycaprolactone composite fibers for controlled magnetic responsive antifungal drug release, Colloids and Surfaces B: Biointerfaces. 145 (2016) 757–767. https://doi.org/10.1016/j.colsurfb.2016.05.092.

[20] J. Meng, B. Xiao, Y. Zhang, J. Liu, H. Xue, J. Lei, H. Kong, Y. Huang, Z. Jin, N. Gu, H. Xu, Super-paramagnetic responsive nanofibrous scaffolds under static magnetic field enhance osteogenesis for bone repair in vivo, Scientific Reports. 3 (2013) 2655. https://doi.org/10.1038/srep02655.

[21] C.J. Mortimer, C.J. Wright, The fabrication of iron oxide nanoparticle-nanofiber composites by electrospinning and their applications in tissue engineering, Biotechnology Journal. 12 (2017) 1600693. https://doi.org/10.1002/biot.201600693.

[22] D. Shan, Y. Shi, S. Duan, Y. Wei, Q. Cai, X. Yang, Electrospun magnetic poly(l-lactide) (PLLA) nanofibers by incorporating PLLA-stabilized Fe3O4 nanoparticles, Materials Science and Engineering: C. 33 (2013) 3498–3505. https://doi.org/10.1016/j.msec.2013.04.040.

[23] C.D.L. Johnson, D. Ganguly, J.M. Zuidema, T.J. Cardinal, A.M. Ziemba, K.R. Kearns, S.M. McCarthy, D.M. Thompson, G. Ramanath, D.A. Borca-Tasciuc, S. Dutz, R.J. Gilbert, Injectable, Magnetically Orienting Electrospun Fiber Conduits for Neuron Guidance, ACS Applied Materials & Interfaces. (2018). https://doi.org/10.1021/acsami.8b18344.

[24] H. Awada, A. Al Samad, D. Laurencin, R. Gilbert, X. Dumail, A. El Jundi, A. Bethry, R. Pomrenke, C. Johnson, L. Lemaire, F. Franconi, G. Félix, J. Larionova, Y. Guari, B. Nottelet, Controlled Anchoring of Iron Oxide Nanoparticles on Polymeric Nanofibers: Easy Access to Core@Shell Organic–Inorganic Nanocomposites for Magneto-Scaffolds, ACS Appl. Mater. Interfaces. 11 (2019) 9519–9529. https://doi.org/10.1021/acsami.8b19099.

[25] A.M. Ziemba, T.D. Fink, M.C. Crochiere, D.L. Puhl, S. Sapkota, R.J. Gilbert, R.H. Zha, Coating Topologically Complex Electrospun Fibers with Nanothin Silk Fibroin Enhances Neurite Outgrowth in Vitro, ACS Biomater. Sci. Eng. 6 (2020) 1321–1332. https://doi.org/10.1021/acsbiomaterials.9b01487.

[26] H.B. Wang, M.E. Mullins, J.M. Cregg, A. Hurtado, M. Oudega, M.T. Trombley, R.J. Gilbert, Creation of highly aligned electrospun poly-L-lactic acid fibers for nerve regeneration applications, J Neural Eng. 6 (2009) 016001. https://doi.org/10.1088/1741-2560/6/1/016001.

[27]   C. Ayres, G.L. Bowlin, S.C. Henderson, L. Taylor, J. Shultz, J. Alexander, T.A. Telemeco, D.G. Simpson, Modulation of anisotropy in electrospun tissue-engineering scaffolds: Analysis of fiber alignment by the fast Fourier transform, Biomaterials. 27 (2006) 5524–5534. https://doi.org/10.1016/j.biomaterials.2006.06.014.

[28]   A.R. D'Amato, D.L. Puhl, A.M. Ziemba, C.D.L. Johnson, J. Doedee, J. Bao, R.J. Gilbert, Exploring the effects of electrospun fiber surface nanotopography on neurite outgrowth and branching in neuron cultures, PLOS ONE. 14 (2019) e0211731. https://doi.org/10.1371/journal.pone.0211731.

[29]   N.J. Schaub, C.L. Beux, J. Miao, R.J. Linhardt, J.G. Alauzun, D. Laurencin, R.J. Gilbert, The Effect of Surface Modification of Aligned Poly-L-Lactic Acid Electrospun Fibers on Fiber Degradation and Neurite Extension, PLOS ONE. 10 (2015) e0136780. https://doi.org/10.1371/journal.pone.0136780.

[30]   E. Amstad, M. Textor, E. Reimhult, Stabilization and functionalization of iron oxide nanoparticles for biomedical applications, Nanoscale. 3 (2011) 2819–2843. https://doi.org/10.1039/C1NR10173K.

[31]   H.B. Wang, M.E. Mullins, J.M. Cregg, C.W. McCarthy, R.J. Gilbert, Varying the diameter of aligned electrospun fibers alters neurite outgrowth and Schwann cell migration, Acta Biomaterialia. 6 (2010) 2970–2978. https://doi.org/10.1016/j.actbio.2010.02.020.

[32]   S.Y. Chew, R. Mi, A. Hoke, K.W. Leong, The Effect of the Alignment of Electrospun Fibrous Scaffolds on Schwann Cell Maturation, Biomaterials. 29 (2008) 653–661. https://doi.org/10.1016/j.biomaterials.2007.10.025.

[33]   C.F. Blackman, S.G. Benane, D.E. House, Evidence for direct effect of magnetic fields on neurite outgrowth, The FASEB Journal. 7 (1993) 801–806. https://doi.org/10.1096/fasebj.7.9.8330687.

[34]   C.-Y. Lin, W.J. Huang, K. Li, R. Swanson, B. Cheung, V.W. Lin, Y.-S. Lee, Differential Intensity-dependent Effects of Magnetic Stimulation on the Longest Neurites and Shorter Dendrites in Neuroscreen-1 Cells, J Neural Eng. 12 (2015) 026013. https://doi.org/10.1088/1741-2560/12/2/026013.

[35]   S. Kim, W.-S. Im, L. Kang, S.-T. Lee, K. Chu, B.I. Kim, The application of magnets directs the orientation of neurite outgrowth in cultured human neuronal cells, Journal of Neuroscience Methods. 174 (2008) 91–96. https://doi.org/10.1016/j.jneumeth.2008.07.005.

[36]   L. Li, G. Yang, J. Li, S. Ding, S. Zhou, Cell behaviors on magnetic electrospun poly-d, l-lactide nanofibers, Materials Science and Engineering: C. 34 (2014) 252–261. https://doi.org/10.1016/j.msec.2013.09.021.

[37]   Y. Wang, S. Du, T. Liu, J. Ren, J. Zhang, H. Xu, H. Zhang, Y. Liu, L. Lu, Schwann Cell Migration through Magnetic Actuation Mediated by Fluorescent–Magnetic Bifunctional Fe3O4·Rhodamine 6G@Polydopamine Superparticles, ACS Chem. Neurosci. 11 (2020) 1359–1370. https://doi.org/10.1021/acschemneuro.0c00116.

[38]   L. Huang, B. Xia, Z. Liu, Q. Cao, J. Huang, Z. Luo, Superparamagnetic Iron Oxide Nanoparticle-Mediated Forces Enhance the Migration of Schwann Cells Across the Astrocyte-Schwann Cell Boundary In vitro, Front. Cell. Neurosci. 11 (2017). https://doi.org/10.3389/fncel.2017.00083.

[39]   B. Xia, L. Huang, L. Zhu, Z. Liu, T. Ma, S. Zhu, J. Huang, Z. Luo, Manipulation of Schwann cell migration across the astrocyte boundary by polysialyltransferase-loaded superparamagnetic nanoparticles under magnetic field, Int J Nanomedicine. 11 (2016) 6727–6741. https://doi.org/10.2147/IJN.S122358.

Appendix A. Supplementary data

Table 1: Materials/product information

Table 2: Equipment information

Figure 1: TEM of SPIONs and diameter

Figure 2: Custom Teflon mold and color change of scaffolds after grafting

Figure 3: TEM of SPION-grafted fiber cross section?
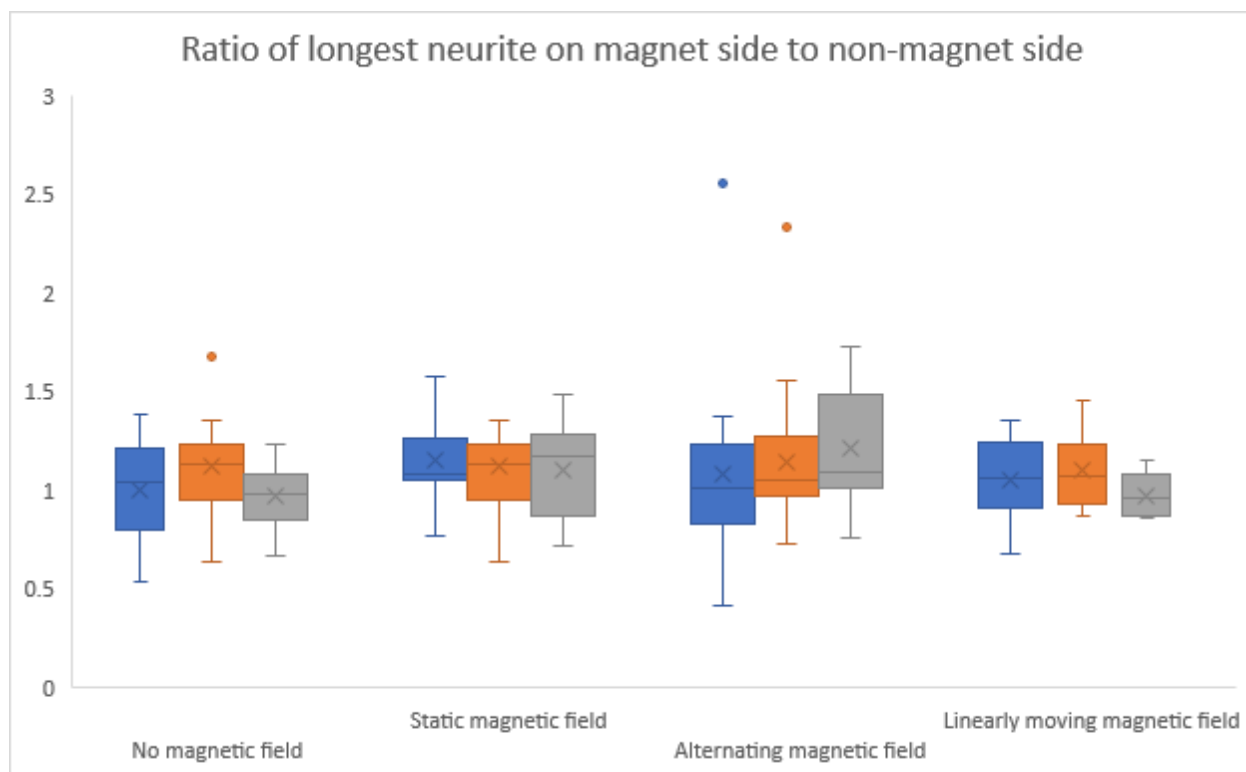
Figure 4: Ratio of longest neurite

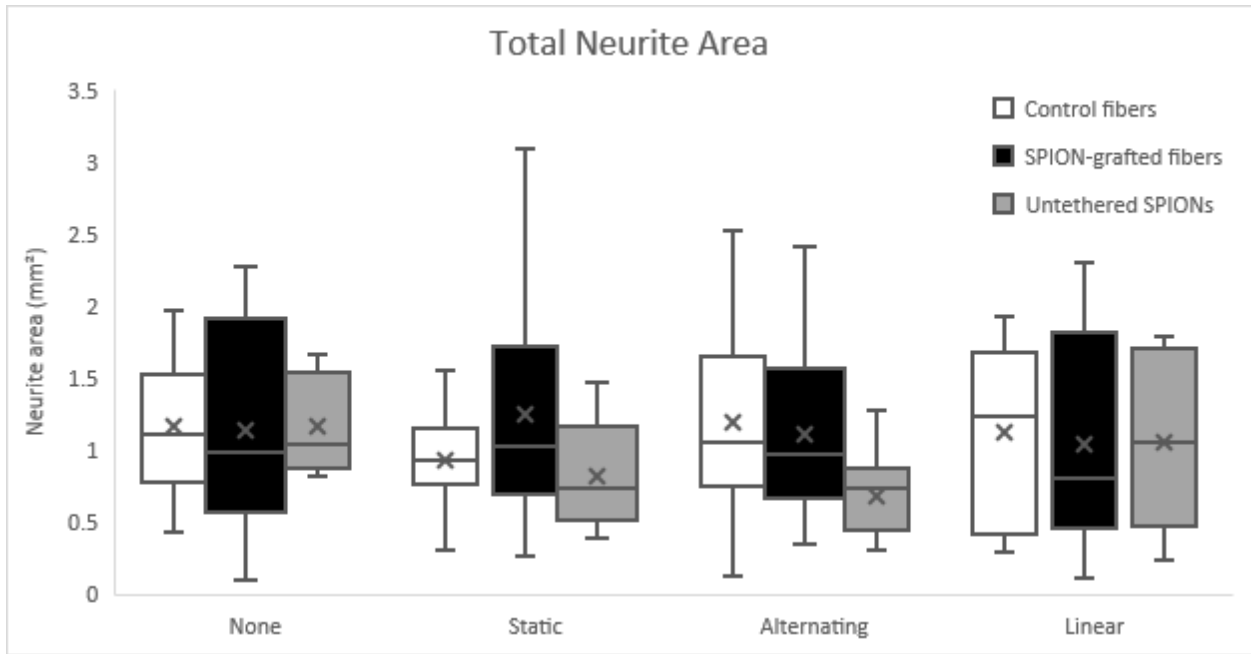Figure 5: Total neurite area boxplot (not separated by side of DRG)

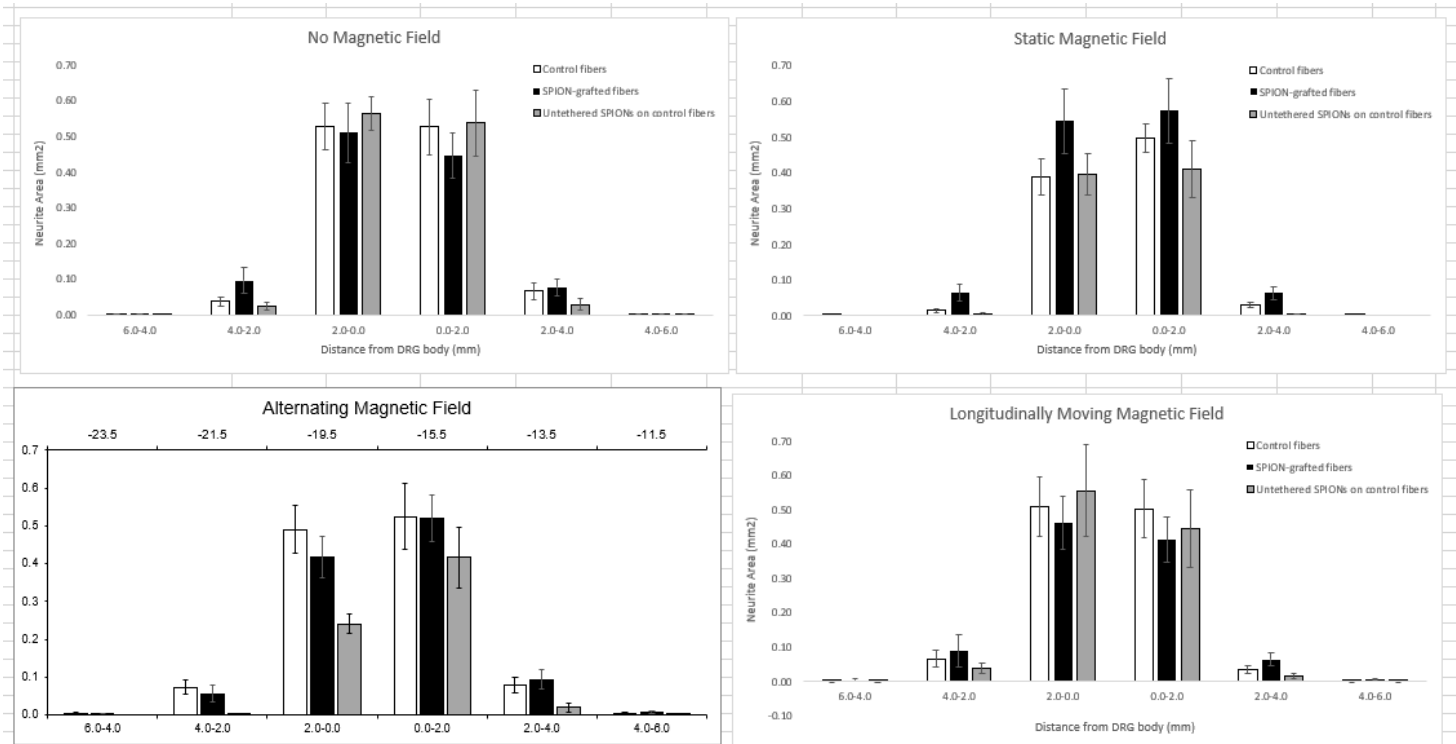Figure 6: Neurite area in binned regions for all magnetic fields

Figure 7: Schwann cell migration in binned regions for all magnetic fields